



38 **ABSTRACT**

39

40       Microcircuits in the neocortex are functionally organized along layers and columns,  
41 which are the fundamental modules of cortical information processing. While the function of  
42 cortical microcircuits has focused on neuronal elements, much less is known about the  
43 functional organization of astrocytes and their bidirectional interaction with neurons. Here  
44 we show that CB<sub>1</sub>R-mediated astrocyte activation by neuron-released endocannabinoids  
45 elevate astrocyte Ca<sup>2+</sup> levels, stimulate ATP/adenosine release as gliotransmitters, and  
46 transiently depress synaptic transmission in layer 5 pyramidal neurons at relatively distant  
47 synapses (>20 μm) from the stimulated neuron. This astrocyte-mediated heteroneuronal  
48 synaptic depression occurred between pyramidal neurons within a cortical column and was  
49 absent in neurons belonging to adjacent cortical columns. Moreover, this form of  
50 heteroneuronal synaptic depression occurs between neurons located in particular layers,  
51 following a specific connectivity pattern that depends on a layer-specific neuron-to-astrocyte  
52 signaling. These results unravel the existence of astrocyte-mediated non-synaptic  
53 communication between cortical neurons, and that this communication is column- and layer-  
54 specific, which adds further complexity to the intercellular signaling processes in the cortex.

## 55 INTRODUCTION

56 The neocortex is the most complex structure of the mammalian brain involved in higher  
57 cognitive functions. The cellular organization of the cerebral cortex is well known since the work  
58 of Cajal and his disciple Lorente de Nó, who proposed that cortical neurons form functional  
59 modules that serve as the “elementary cortical unit of operation”<sup>1,2</sup>. Cortical neurons are  
60 organized horizontally in six layers and vertically in columns<sup>3</sup>. The columnar configuration of  
61 the neocortex is a widely accepted idea explaining its functional organization<sup>4,5</sup>. A great amount  
62 of information has been provided regarding the neuronal elements involved in cortical circuits  
63 and their synaptic microorganization<sup>6</sup>. However, the properties of non-neuronal cell types, like  
64 astrocytes, and their functional interactions with neurons in this elementary module remain  
65 largely unexplored.

66 Astrocytes have emerged as key regulatory elements of synapses, responding with  $\text{Ca}^{2+}$   
67 elevations to synaptically-released neurotransmitters and releasing gliotransmitters that regulate  
68 synaptic transmission in different brain areas<sup>7-9</sup>. In the cortex, sensory stimuli or direct neuronal  
69 stimulation evoke astrocyte  $\text{Ca}^{2+}$  elevations<sup>10-17</sup>, which are topographically represented in the  
70 primary somatosensory cortex S1<sup>18</sup> and spatially restricted to the cortical columns in the  
71 barrel cortex<sup>14</sup>. Cortical astrocyte  $\text{Ca}^{2+}$  elevations can, in turn, stimulate the release of  
72 gliotransmitters, such as glutamate or D-Serine, that can regulate synaptic transmission<sup>13,15</sup>, and  
73 that can be responsible for the observed astrocyte-mediated regulation of the cortical network  
74 function<sup>17,19-21</sup>. Moreover, synaptic regulation by astrocytes may be exerted at synapses  
75 relatively distant from the active synapses<sup>22-24</sup>. This phenomenon, termed lateral astrocyte  
76 synaptic regulation<sup>25</sup>, resembles the classical heterosynaptic modulation but is mechanistically  
77 dissimilar because it involves astrocytes and may be crucial in brain circuits where spatial  
78 signaling greatly influences neural network function, like the neocortical columns. However, the  
79 spatial properties of astrocyte-neuron interaction and the consequent synaptic regulation in  
80 defined cortical columns and layers remain unidentified.

81 Endocannabinoid (eCB) signaling has been proposed to mediate astrocyte-neuron  
82 communication in different brain regions, including the neocortex. In particular, endogenous  
83 activation of astroglial type-1 cannabinoid receptors ( $\text{CB}_1\text{Rs}$ ) regulates hippocampal and  
84 neocortical synaptic transmission and plasticity<sup>15,22,26,27</sup>. Here, in order to decipher the regulatory  
85 role of astrocytes in the synaptic physiology of cortical columns, we took advantage of this eCB  
86 signaling to physiologically stimulate cortical astrocytes. We show that eCBs released from

87 layer 5 (L5) pyramidal neurons induce  $\text{Ca}^{2+}$  elevations in astrocytes and transiently depressed  
88 synaptic transmission in adjacent pyramidal neurons. This form of heteroneuronal synaptic  
89 depression required astrocytic cannabinoid receptor type ( $\text{CB}_1\text{R}$ ) activation and was  
90 mediated by presynaptic type 1 adenosine receptors ( $\text{A}_1\text{Rs}$ ). Astrocyte-mediated  
91 heteroneuronal synaptic depression was present between pyramidal neurons within a cortical  
92 column and was absent in neurons belonging to adjacent cortical columns. Moreover, this  
93 form of heteroneuronal synaptic depression occurred between neurons located in particular  
94 layers, following a specific connectivity pattern that depends on a layer-specific neuron-to-  
95 astrocyte signaling. These results reveal the existence of astrocyte-mediated non-synaptic  
96 communication between cortical neurons, which is column- and layer-specific, and which  
97 adds further complexity to the intercellular signaling processes in the cortex.

## 98 RESULTS

99

### 100 Endocannabinoid signaling induces homoneuronal and heteroneuronal synaptic 101 depression in S1

102 To investigate the spatial regulation of synaptic transmission in the primary  
103 somatosensory cortex, we performed double patch-recordings of layer 5 (L5) pyramidal  
104 neurons and monitored excitatory postsynaptic currents (EPSCs) evoked by electrical  
105 stimulation of layer 2/3 (L2/3). We then stimulated one neuron by a depolarizing pulse and  
106 recorded synaptic currents in both the “stimulated” neuron (homoneuronal synapses) and the  
107 adjacent (70-270  $\mu\text{m}$  apart) “nonstimulated” neuron (heteroneuronal synapses) (**Figures 1A**  
108 **and 1B**). Stimulation of single L5 pyramidal neurons induced a transient synaptic depression  
109 in 36 out of 93 (38.7%) homoneuronal synapses. Furthermore, in simultaneously recorded  
110 heteroneuronal synapses, this neuronal depolarization (ND) also induced a transient  
111 depression of synaptic transmission in 20 out of 72 (27.8%) heteroneuronal synapses  
112 (**Figures 1C-E**). Both homoneuronal and heteroneuronal synaptic depressions could be  
113 reliably induced by repeated stimulations (**Figure S1A and S1B**) and were associated with  
114 changes in the paired-pulse ratio (PPR), which are consistent with presynaptic mechanisms  
115 (**Figures S1C and S1D**).

116 ND is known to trigger the release of eCBs<sup>28,29</sup> that can directly affect relatively close  
117 synapses ( $\sim 20 \mu\text{m}$ )<sup>29-32</sup>, a phenomenon called depolarization-induced suppression of  
118 excitation (DSE)<sup>29-34</sup>, and indirectly regulate more distant synapses through stimulation of  
119 astrocytes<sup>15,22,27</sup>, a phenomenon called astrocyte-mediated lateral regulation of synaptic  
120 transmission. Consistent with eCB-mediated synaptic regulation, homoneuronal and  
121 heteroneuronal synaptic depressions observed under control conditions were abolished  
122 following bath perfusion with the cannabinoid receptor type 1 (CB<sub>1</sub>R) antagonist AM251 (2  
123  $\mu\text{M}$ ; n = 12 and 6), indicating that both phenomena were mediated by CB<sub>1</sub>R activation  
124 (**Figures 1D and 1E**).

125 We then tested whether these phenomena were present in other cortical layers by  
126 performing paired recordings of neurons in L2/3 and L4. L2/3 or L4 ND induced both  
127 homoneuronal (14 out of 38 and 8 of 32 pairs; 36.8% and 25%, respectively) and  
128 heteroneuronal (14 out of 39 and 8 of 27 pairs; 35.9% and 29.6%, respectively) depression

129 (Figures 1F-I), indicating that eCB-induced homoneuronal and heteroneuronal synaptic  
130 depressions are a general cortical phenomena.

131

### 132 **Heteroneuronal, but not homoneuronal, synaptic depression requires endocannabinoid** 133 **signaling in astrocytes**

134 We then investigated the role of astrocyte CB<sub>1</sub>Rs on the eCB-induced homoneuronal and  
135 heteroneuronal synaptic depression. We selectively deleted CB<sub>1</sub>R expression in cortical  
136 astrocytes by expressing Cre-recombinase under the control of the astroglial promoter GFAP,  
137 using local injection of AAV8-GFAP-mCherry-Cre in S1 of CB<sub>1</sub>R<sup>flox/flox</sup> mice (Figure 2A).  
138 These mice are herein termed aCB<sub>1</sub>R<sup>-/-</sup> mice, and their controls, termed aCB<sub>1</sub>R mice, were  
139 CB<sub>1</sub>R<sup>flox/flox</sup> mice injected with AAV8-GFAP-mCherry (i.e., lacking Cre). To assess the  
140 efficacy of the approach, we monitored the CB<sub>1</sub>R-mediated astrocyte Ca<sup>2+</sup> responses to the  
141 CB<sub>1</sub>R agonist WIN 55,212-2 (300 μM) using two-photon microscopy and the genetically  
142 encoded calcium indicator GCaMP6f selectively expressed in astrocytes via injection of  
143 AAV5-gfaABC1D-cyto-GCaMP6f in S1 (Figure 2D). While the astrocyte Ca<sup>2+</sup> activity,  
144 quantified from the Ca<sup>2+</sup> event probability, was increased by local application of WIN  
145 55,212-2 in control aCB<sub>1</sub>R mice (n = 190 astrocytes from 13 slices), the WIN-evoked  
146 responses were significantly reduced in aCB<sub>1</sub>R<sup>-/-</sup> mice (n = 261 astrocytes from 14 slices;  
147 Figure 2D-F), confirming the suitability of the viral approach to delete CB<sub>1</sub>R signaling in  
148 astrocytes.

149 Next, we tested the impact of astroglial deletion of CB<sub>1</sub>Rs on the ND-evoked  
150 homoneuronal and heteroneuronal synaptic depression in L5. Accordingly, the homoneuronal  
151 depression was not affected in mice lacking CB<sub>1</sub>Rs in astrocytes (12 out of 35 cells; 34.3%)  
152 (Figures 2B and 2C). By contrast, the heteroneuronal synaptic depression was absent in  
153 aCB<sub>1</sub>R<sup>-/-</sup> mice (0 out of 27 cells; 0%) (Figures 2B and 2C). These results indicate that eCB-  
154 induced heteroneuronal, but not homoneuronal, synaptic depression involves CB<sub>1</sub>R signaling  
155 in astrocytes.

156

### 157 **Heteroneuronal synaptic depression requires astrocyte Ca<sup>2+</sup> signaling and activation of** 158 **presynaptic A1 receptors**

159  $\text{Ca}^{2+}$  elevations in astrocytes evoked by different neurotransmitters, including  
160 eCBs<sup>22,35,36</sup>, are known to stimulate the release of gliotransmitters that regulate synaptic  
161 function (e.g.,<sup>15,22,35–37</sup>). Hence, we investigated whether the homoneuronal and  
162 heteroneuronal synaptic depressions depended on the astrocytic  $\text{Ca}^{2+}$  signal. We depolarized  
163 L5 pyramidal neurons using the approach that elicits homoneuronal and heteroneuronal  
164 synaptic depression as indicated above and monitored the astrocyte  $\text{Ca}^{2+}$  activity using  
165 GCaMP6f selectively expressed in astrocytes (**Figure 2D**). To isolate eCB-induced effects,  
166 experiments were performed in the presence of a cocktail of antagonists of glutamatergic,  
167 GABAergic, purinergic, and cholinergic receptors (see Material and Methods). Under these  
168 conditions, ND elevated astrocyte  $\text{Ca}^{2+}$  fluctuations (n = 142 astrocytes of 6 slices), an effect  
169 that was abolished in the presence of AM251, indicating that these responses were mediated  
170 by CB<sub>1</sub>R activation (n = 122 astrocytes of 6 slices; **Figures 3A and 3B**).

171 Moreover, ND-evoked astrocyte  $\text{Ca}^{2+}$  elevations were largely absent in inositol-1,4,5-  
172 trisphosphate (IP<sub>3</sub>)-receptor type 2-deficient mice (IP<sub>3</sub>R<sub>2</sub><sup>-/-</sup> mice), in which G protein-  
173 mediated  $\text{Ca}^{2+}$  signal is selectively impaired in astrocytes<sup>27,38–40</sup> (n = 164 astrocytes of 11  
174 slices; **Figures 3A and 3B**). In these mice, the homoneuronal depression was preserved (13  
175 out of 30 cases; 43.3%), but the heteroneuronal depression was absent (0 out of 17 cases;  
176 0%) (**Figure 3C**). Collectively these results indicate that the astrocyte  $\text{Ca}^{2+}$  signal is required  
177 for the heteroneuronal, but not the homoneuronal, synaptic depression.

178 We then investigated the gliotransmitter responsible for the heteroneuronal depression.  
179 ATP and its metabolic product adenosine are known to be released by astrocytes<sup>8</sup> and to  
180 regulate synaptic transmission in several brain areas<sup>23,24,36,37,41,42</sup>. Therefore, we hypothesized  
181 that eCB-induced astrocyte calcium elevations would stimulate the release of ATP/adenosine  
182 that acting on neuronal type 1 adenosine receptors (A<sub>1</sub>Rs) would depress synaptic  
183 transmission. To test this idea, we depolarized L5 pyramidal neurons and monitored the  
184 homo- and heteroneuronal synaptic depression before and after bath application of the A<sub>1</sub>R  
185 antagonist CPT (5  $\mu\text{M}$ ). While the homoneuronal depression was unaffected (n = 8), the  
186 heteroneuronal depression was abolished in the presence of CPT (n = 8; **Figure 3C**).  
187 Consistent with results observed in L5, heteroneuronal depressions in L4 and L2/3 were also  
188 abolished by the A<sub>1</sub>R antagonist CPT (**Figure 3D**).

189 To further test the astrocyte involvement, we investigated if activation of G-protein-  
190 mediated signaling in astrocytes depresses excitatory transmission in the S1 cortex by  
191 directly and selectively activating astrocytes using designer receptors exclusively activated  
192 by designed drugs (DREADDs). Astrocytes in the S1 cortex were targeted with AAV8-  
193 GFAP-Gq-DREADD-mCherry and AAV5-gfaABC1d-GCaMP6f (**Figure 3E**). Activation of  
194 Gq-DREADDs with the synthetic agonist clozapine-N-oxide (CNO, 1 mM) delivered from  
195 a micropipette by pressure pulses (5 s) (**Figure 3E**) induced  $\text{Ca}^{2+}$  elevations in astrocytes ( $n$   
196 = 253 astrocytes from 14 slices, **Figure 3G**) and depressed synaptic transmission in L5  
197 pyramidal neurons ( $n = 11$ ; **Figure 3F**), which was associated with an increase in PPR  
198 indicating a presynaptic mechanism ( $n = 11$ ; **Figure S1E**). Moreover, in the presence of CPT,  
199 CNO also induced  $\text{Ca}^{2+}$  elevations in astrocytes ( $n = 87$  astrocytes from 7 slices, **Figure 3G**)  
200 but failed to affect synaptic transmission ( $n = 7$ , **Figure 3F**). In slices from mice that were  
201 injected with control AAV8-GFAP-mCherry virus (i.e., lacking DREADDs), CNO  
202 application failed to affect both synaptic transmission ( $n = 11$ ; **Figure 3F**) and astrocyte  
203  $\text{Ca}^{2+}$  dynamics ( $n = 92$  astrocytes from 8 slices; **Figure 3G**). These results suggest that  
204 astrocyte  $\text{Ca}^{2+}$  elevations are sufficient to regulate cortical synaptic transmission.

205

206 Taking together, these results indicate that neuron-released eCBs induce homeoneuronal  
207 depression by directly acting on neuronal  $\text{CB}_1\text{Rs}$ . Concomitantly, eCBs activate  $\text{CB}_1\text{Rs}$  in  
208 astrocytes, elevate their intracellular  $\text{Ca}^{2+}$ , and stimulate the release of ATP/Adenosine,  
209 which acts on presynaptic  $\text{A}_1\text{Rs}$  triggering the heteroneuronal depression (**Figure 3H**).

210

### 211 **Astrocyte-mediated heteroneuronal depression is column-specific**

212 The functional properties of the somatosensory cortex rely on their modular organization,  
213 comprising sub-circuits of layer connectivity within cortical columns<sup>3,5,6</sup>. Thus, we  
214 investigated whether the astrocyte-mediate heteroneuronal depression was also spatially  
215 restricted to a single column. We analyzed this phenomenon in the somatosensory barrel  
216 cortex, where cortical columns can be easily identified (**Figure 4A**). We performed paired  
217 whole-cell recordings of L4 neurons located at a similar distance (70-270  $\mu\text{m}$ ) but either  
218 within the same or in adjacent columns (**Figure 4A**). Depolarization of a single L4 neuron to  
219 stimulate eCBs release induced heteroneuronal depression in the paired recorded neuron



220 located in the same column (10 out of 29 paired recordings; 35%, **Figure 4B**). Consistent  
221 with the mechanistic interpretation described above, this phenomenon was blocked after CPT  
222 perfusion (**Figure S1G**). In contrast to this intracolumn regulation, the heteroneuronal  
223 regulation was absent in neurons located at a similar distance but in an adjacent cortical  
224 column (0 out 15 paired recordings; 0%, **Figure 4C**). In both cases, intra- and intercolumn  
225 recordings displayed homoneuronal synaptic depression (16 out 48 cells; 33%, **Figure S1F**).

226

227 Overall, these results indicate that the eCB-induced astrocyte-mediated heteroneuronal  
228 synaptic regulation is column-specific, i.e., it is not a wide unspecific phenomenon but a  
229 synaptic regulatory signaling that specifically occurs between cells located within a cortical  
230 column.

231

### 232 **Astrocyte-mediated heterosynaptic depression is layer-specific**

233 Cortical information processing depends not only on the columnar organization but also  
234 on the functional interaction across different layers<sup>6</sup>. Therefore, we examined the functional  
235 organization of heteroneuronal and homoneuronal synaptic depression across different  
236 cortical layers, i.e., between neurons located in L2/3, L4, and L5 (**Figure 5**). We performed  
237 paired recordings of neurons in these layers, depolarized one neuron to stimulate eCB release,  
238 and monitored EPSCs in the other neuron located in another layer. While depolarizing a  
239 single L2/3 neuron did not affect synaptic transmission in L4 neurons (n = 11) (**Figures 5A**  
240 **and 5B**), stimulation of a single L4 neuron induced heteroneuronal synaptic depression in  
241 L2/3 neurons (5 out of 10 cases; 50%, **Figures 5A and B**). Likewise, stimulation of a single  
242 L2/3 neuron did not alter synaptic transmission in L5 neurons (n = 8; **Figures 5C and 5D**),  
243 but stimulation of L5 neurons induced heteroneuronal depression in L2/3 neurons (4 out of  
244 10 cases; 40%, **Figures 5C and 5D**). Finally, stimulation of L4 neurons depressed  
245 neurotransmission in L5 pyramidal neurons (4 out of 14 cases; 28.1%, **Figures 5E and 5F**),  
246 but L5 neuron stimulation did not impact synaptic transmission in L4 neurons (n = 16;  
247 **Figures 5E and 5F**). In summary, astrocyte-mediated heteroneuronal depression occurs  
248 between neurons located in different layers, but following a specific pattern and not  
249 necessarily reciprocally. For example, synapses in L2/3 neurons can be regulated by neurons

250 located in L4 or L5, but not vice versa; and L4 neurons can regulate neurons in L2/3 and L5  
251 but are not regulated by them.

252 Together, these results indicate that eCB-induced astrocyte-mediated heteroneuronal  
253 synaptic regulation is not an unspecific phenomenon, rather it is layer-specific, selectively  
254 occurring among neurons following a layer-specific pattern (**Figure 5G**).

### 255 256 **Astrocytic calcium responses to eCBs are not homogeneous across cortical layers**

257 Because the heteroneuronal depression depends on the eCB-induced astrocyte  
258  $\text{Ca}^{2+}$  signals, its layer-specificity might be accounted for by layer-specificity of astrocyte  
259 responsiveness to eCBs (**Figure 6A**). To test this idea, we examined the astrocyte  
260  $\text{Ca}^{2+}$  signals in different layers in response to eCBs released by depolarization of neurons.  
261 To ensure that the astrocyte activation was due to eCBs, we performed the experiments in  
262 the presence of TTX (1  $\mu\text{M}$ ) and the cocktail of neurotransmitter receptor antagonists (see  
263 Material and Methods). Neuronal depolarization of L2/3, L4 or L5 neurons elevated  
264 intracellular  $\text{Ca}^{2+}$  in astrocytes located within the same layer (n = 110 astrocytes from 5 slices;  
265 n = 110 astrocytes from 4 slices; n = 142 from 6 slices respectively). These responses were  
266 abolished by AM251, confirming to be the result of eCB signaling (n = 89 astrocytes from 5  
267 slices; n = 79 astrocytes from 4 slices; n = 122 from 6 slices respectively, **Figures 6B-D**).

268 We then examined the astrocyte responses to neuron-released eCBs across cortical  
269 layers. Stimulation of L2/3 neurons increased the astrocyte  $\text{Ca}^{2+}$  event probability in L2/3 (n  
270 = 185 astrocytes from 10 slices) but failed to increase  $\text{Ca}^{2+}$  signaling in L4 (n = 62 astrocytes  
271 from 5 slices) or L5 (n = 129 astrocytes from 6 slices) astrocytes (**Figure 6E**). Likewise,  
272 stimulation of L4 neurons elevated  $\text{Ca}^{2+}$  in L4 (n = 163 astrocytes from 8 slices), L5 (n = 87  
273 astrocytes from 7 slices) and L2/3 (n = 71 astrocytes from 6 slices) astrocytes (**Figure 6F**).  
274 Finally, stimulation of L5 neurons produced an increase in the  $\text{Ca}^{2+}$  event probability in L5  
275 (n = 267 astrocytes from 13 slices) and L2/3 (n = 202 astrocytes from 8 slices) astrocytes but  
276 not in L4 (n = 144 astrocytes from 8 slices) astrocytes (**Figure 6G**). These results indicate  
277 that astrocyte  $\text{Ca}^{2+}$  increases mediated by eCBs signaling obeys a layer-specific pattern in  
278 agreement with the astrocyte-mediated heterosynaptic regulation produced by neuronal  
279 depolarization (**Figure 6H**).

280

281        In summary, eCB-mediated neuron-to-astrocyte signaling is a form of communication  
282 that occurs between cells that can be located in different layers, but following a specific  
283 connectivity pattern. Like the heteroneuronal depression, this specific pattern does not  
284 necessarily involve reciprocal signaling between layers. Notably, the specific neuron-to-  
285 astrocyte connectivity pattern mirrors the heteroneuronal depression pattern, suggesting that  
286 the selective neuron-astrocyte signaling between layers is responsible for the astrocyte-  
287 mediated non-synaptic communication between neurons in different cortical layers.

288 **DISCUSSION**

289

290 Present results show that astrocytes regulate cortical synaptic function in a layer- and  
291 column-specific manner and that the functional interaction between cortical astrocytes and  
292 synapses is highly spatially organized. We show that activation of astrocytes by endogenous  
293 stimuli –eCBs physiologically released from cortical neurons–, induced astrocyte  $\text{Ca}^{2+}$   
294 elevations and transiently depressed synaptic transmission in neurons located in the same and  
295 distinct cortical layers. This heteroneuronal synaptic depression requires astrocytic  $\text{CB}_1\text{R}$   
296 activation, is mediated by activation of presynaptic  $\text{A}_1$  receptors, and can be mimicked by  
297 astrocyte-specific chemogenetic stimulation. Additionally, our results also show that neuron-  
298 released eCBs can depress synaptic transmission by directly activating  $\text{CB}_1\text{Rs}$  in  
299 homoneuronal synapses, a phenomenon known as DSE<sup>29–34</sup>.

300 The neocortex is highly organized in layers and columns with precisely neuronal  
301 connectivity. Our results indicate that eCB-mediated astrocyte-neuron signaling is also  
302 exquisitely organized. First, the astrocyte-mediated heteroneuronal depression was found to  
303 be column-specific because it only occurred between neurons located within the same  
304 column and not between neurons located at similar distances but in adjacent columns (**Figure**  
305 **4**). Second, astrocyte-mediated heteroneuronal regulation occurred between neurons located  
306 in different layers, but according to a specific connectivity pattern (**Figure 5**). Third, the  
307 eCB-mediated neuron-to-astrocyte signaling was also layer-specific because astrocytic  
308 calcium responses to eCBs released by neurons in different cortical layers were not  
309 homogeneous across the cortical layers; rather neuron-to-astrocyte signaling occurred  
310 according to particular signaling patterns (**Figure 6**).

311 Several previous studies have shown that astrocytes stimulated by eCBs lead to  
312 regulation of synaptic transmission in diverse brain areas, including the hippocampus,  
313 amygdala, and neocortex<sup>15,22,26,27</sup>. In the neocortex, synapses onto layer 2/3 neurons undergo  
314 spike-timing long-term depression (LTD) mediated by glutamate released from astrocytes<sup>15</sup>.  
315 By contrast, we found (**Figures 1, 2, and 3**) that eCB-induced astrocyte activation transiently  
316 depresses synapses through ATP/adenosine release as gliotransmitters. Different neuronal  
317 stimulating paradigms used in these studies may account for such discrepancies. As a matter  
318 of fact, astrocytes are competent to release distinct gliotransmitters depending on the pattern  
319 of neuronal stimulation as demonstrated in the hippocampus, where astrocytes can release

320 glutamate upon low frequency stimulation of neighboring interneurons or glutamate and  
321 ATP/adenosine upon high frequency stimulation<sup>43</sup>.

322 The eCB-induced astrocyte-mediated heteroneuronal depression was found to be  
323 restricted within a single cortical column, supporting the idea of a highly organized signaling  
324 between astrocytes and neurons at a modular level. These results agree with previous reports  
325 showing that astrocyte Ca<sup>2+</sup> signal is spatially restricted in astrocytes located within the  
326 columns of the barrel cortex<sup>14,44,45</sup>. The column-specific astrocyte-mediated synaptic  
327 regulation also indicates that astrocyte-neuron networks are functionally organized obeying  
328 the columnar organization of the neuronal connectivity pattern.

329 In conclusion, the present data indicate that astrocytes modulate cortical synaptic  
330 transmission in a column and layer-specific manner, obeying the structural and functional  
331 organization of the cortex, which suggests that they are an integral part of the cortical  
332 modules. Moreover, astrocytes, by providing layer-specific signaling pathways of non-  
333 synaptic communication between neurons, add further complexity to the signaling  
334 mechanisms underlying cortical network function. This finely controlled astrocyte-synapse  
335 interaction is particularly significant in the neocortex, where the spatial integration of  
336 synaptic signals is highly relevant for cortical information processing.

## 337 **METHODS**

338

### 339 **Ethics statement**

340 All of the procedures for handling and sacrificing animals were approved by the  
341 University of Minnesota Institutional Animal Care and Use Committee (IACUC) in  
342 compliance with the National Institutes of Health guidelines for the care and use of laboratory  
343 animals.

344

### 345 **Animals**

346 Mice were housed under 12/12-h light/dark cycle, up to five animals per cage, at  
347 temperatures between 68–74°F at 30–70% humidity with freely available food and water.  
348 The following animals (males and females) were used for the present study C57BL/6J, IP<sub>3</sub>R<sub>2</sub><sup>-</sup>  
349 <sup>-</sup> (generously donated by Dr. J Chen), and CB<sub>1</sub>R<sup>fl/fl</sup> 46,47. Adult (≥8 weeks) mice were used.

350

### 351 **Somatosensory Cortex Slice Preparation**

352 Mice were euthanized by decapitation and brains were rapidly removed and placed in  
353 ice-cold artificial cerebrospinal fluid (ACSF). Three-hundred and fifty-micrometer coronal  
354 brain slices containing the somatosensory cortex were prepared via a Leica VT1200  
355 vibratome in a 4°C ACSF solution. Following cutting, slices were allowed to recover in  
356 ACSF containing (in mM): NaCl 124, KCl 2.69, KH<sub>2</sub>PO<sub>4</sub> 1.25, MgSO<sub>4</sub> 2, NaHCO<sub>3</sub> 26, CaCl<sub>2</sub>  
357 2 and glucose 10, gassed with 95% O<sub>2</sub>/5% CO<sub>2</sub> (pH = 7.3) at 31°C for 30 min followed by  
358 30 min at 20–22°C before recording. After a 1 h recovery period, slices were kept at 20–22°C  
359 for the rest of the recording day. Slices were then transferred to an immersion recording  
360 chamber and superfused at 2 ml/min with gassed ACSF and the temperature of the bath  
361 solution was kept at 34°C with a temperature controller TC-324B (Warner Instruments Co.).  
362 Cells were visualized using infrared-differential interference contrast optics (Nikon Eclipse  
363 E600FN, Tokyo, Japan) and 40x water immersion lens. L2/3, L4, and L5 from the forelimb  
364 and hindlimb somatosensory cortex and the barrel subfields were identified with a 10x  
365 objective.

366

### 367 **Electrophysiology**

368 Neurons were selected based on their location, morphology, and firing pattern.  
369 Simultaneous dual electrophysiological recordings from layers 2/3, 4, and 5 pyramidal  
370 neurons were made using the whole-cell-patch-clamp technique. When filled with an internal  
371 solution containing (in mM): KGluconate 135, KCl 10, HEPES 10, MgCl<sub>2</sub> 1, ATP-Na<sub>2</sub> 2 (pH  
372 = 7.3) patch electrodes exhibited a resistance of 3-10 MΩ. All recordings were performed  
373 using PC-ONE amplifiers (Dagan Instruments, Minneapolis, MN). Fast and slow whole-cell  
374 capacitances were neutralized, and series resistance was compensated (~70%), and the  
375 membrane potential was held at -70 mV. Intrinsic electrophysiological properties were  
376 monitored at the beginning and the end of the experiments. Series and input resistances were  
377 monitored throughout the experiment using a -5 mV pulse. Recordings were considered  
378 stable when the series and input resistances, resting membrane, and stimulus artifact duration  
379 did not change > 20%. Furthermore, I-V curves and firing patterns at the beginning and the  
380 end of the experiments were similar. Recordings that did not meet these criteria were  
381 discarded. Signals were fed to a Pentium-based PC through a DigiData 1322A interface  
382 board. Signals were filtered at 1 kHz and acquired at a 10 kHz sampling rate using a DigiData  
383 1322A data acquisition system and pCLAMP 10.3 software (Molecular Devices, San Jose,  
384 CA). Distance of the somas of the paired recorded neurons within a layer varied from, 70-  
385 270 μm. In paired recordings across layers 2/3, 4, and 5, neurons were selected following the  
386 same vertical axis.

387

### 388 **Synaptic Stimulation**

389 Theta capillaries (2-5 μm tip) filled with ACSF were used for bipolar stimulation. The  
390 electrodes were connected to a stimulator S-900 through an isolation unit and placed in L2/3.  
391 When indicated, the stimulation electrode was placed in L4. Paired pulses of 1 ms duration  
392 and 50 ms interval were continuously delivered at 0.33 Hz. Excitatory postsynaptic currents  
393 (EPSCs) were isolated using picrotoxin (50 μM) and CGP5462 (1 μM) to block GABA<sub>A</sub>R  
394 and GABA<sub>B</sub>R, respectively. EPSC amplitude was determined as the peak current amplitude  
395 (2–20 ms after stimulus) minus the mean baseline current (10-30 ms before stimulus). The  
396 paired-pulse ratio (PPR) was estimated as  $PPR = (2^{nd} \text{ EPSC} / 1^{st} \text{ EPSC})$ .

397 To induce eCB release, pyramidal neurons were depolarized from -70 mV to 0 mV for  
398 5 s (ND)<sup>28,29</sup>. Synaptic parameters were determined from 60 stimuli before (basal) and

399 following ND. Baseline mean EPSC amplitude was obtained by averaging mean values  
400 obtained within 3 min of baseline recordings and mean EPSC amplitudes were normalized  
401 to baseline. The ND was applied 2.5 s after the last basal delivered pulse, and no pulses were  
402 presented during the ND. Immediately after the ND was finished, the 0.33-Hz pulse protocol  
403 was restarted. To illustrate the time course of ND-induced effects, synaptic parameters were  
404 grouped in 15 s bins. Three consecutive responses to ND were averaged. A response was  
405 considered a depression if the amplitude of the current was  $< 2$  times the standard deviation  
406 of the baseline current during the first 45 s after ND and was verified by visual inspection.

407 The effects of pharmacological agents (CPT 5  $\mu\text{M}$  and AM251 2  $\mu\text{M}$ ) were tested after  
408 10 min bath perfusion and in the same neurons that previously were depolarized in control  
409 conditions. In all cases the effects of pharmacological agents were tested at  $< 40$  min after  
410 entering whole-cell mode in the stimulating neuron.

411

#### 412 **Ex vivo two-photon calcium fluorescence imaging and electrophysiology**

413 Two-photon microscopy imaging was performed using a Leica SP5 multi-photon  
414 microscope (Leica Microsystems, USA) controlled by the Leica LAS software and adapted  
415 to perform electrophysiological recordings. C57BL/6J,  $\text{IP}_3\text{R}_2^{-/-}$  and  $\text{aCB}_1\text{R}$  mice injected into  
416 S1 with AAV5-GfaABC1d-GCaMP6f and AAV8-GFAP-mCherry were used (for  $\text{aCB}_1\text{R}^{-/-}$   
417 instead AAV8-GFAP-mCherry we used AAV8-GFAP-mCherry-Cre). All  $\text{Ca}^{2+}$  experiments,  
418 except those in which synaptic transmission was recorded, were performed in the presence  
419 of TTX (1  $\mu\text{M}$ ) and a cocktail of neurotransmitter receptor antagonists containing: CNQX  
420 (20  $\mu\text{M}$ ), AP5 (50  $\mu\text{M}$ ), MPEP (50  $\mu\text{M}$ ), LY367385 (100  $\mu\text{M}$ ), picrotoxin (50  $\mu\text{M}$ ), CGP5462  
421 (1  $\mu\text{M}$ ), atropine (50  $\mu\text{M}$ ), CPT (5  $\mu\text{M}$ ), flupenthixol (30  $\mu\text{M}$ ), and suramin (100  $\mu\text{M}$ ).

422 Videos were obtained at  $512 \times 512$  resolution with a sampling interval of 1 s. Red and  
423 green fluorescence was obtained in parallel to match red mCherry-stained astrocyte structure  
424 with green GCaMP6f astrocyte calcium. A custom MATLAB program (Calsee:  
425 <https://www.araquelab.com/code/>) was used to quantify fluorescence level measurements in  
426 astrocytes.  $\text{Ca}^{2+}$  variations recorded at the soma and processes of the cells were estimated as  
427 changes of the fluorescence signal over baseline ( $\Delta F/F_0$ ), and cells were considered to show  
428 a  $\text{Ca}^{2+}$  event when the  $\Delta F/F_0$  increase was at least two times the standard deviation of the  
429 baseline.



430 The astrocyte  $\text{Ca}^{2+}$  signal was quantified from the  $\text{Ca}^{2+}$  event probability, which was  
431 calculated from the number of  $\text{Ca}^{2+}$  elevations grouped in 5 s bins recorded from 8-50  
432 astrocytes per field of view (layer 2/3, 4 or 5 of S1). The time of occurrence was considered  
433 at the onset of the  $\text{Ca}^{2+}$  event. For each astrocyte analyzed, values of 0 and 1 were assigned  
434 for bins showing either no response or a  $\text{Ca}^{2+}$  event, respectively, and the  $\text{Ca}^{2+}$  event  
435 probability was obtained by dividing the number of astrocytes showing an event at each time  
436 bin by the total number of monitored astrocytes<sup>22</sup>. All the astrocytes that showed a  $\text{Ca}^{2+}$  event  
437 during the experiment were used for the analysis. The calcium event probability was  
438 calculated in each slice, and for statistical analysis, the sample size corresponded to the  
439 number of slices as different slices were considered as independent variables. To examine  
440 the difference in  $\text{Ca}^{2+}$  event probability in distinct conditions, the basal  $\text{Ca}^{2+}$  event probability  
441 (mean of the 30 s before a stimulus) was averaged and compared to the average  $\text{Ca}^{2+}$  event  
442 probability (5 s after a stimulus). For ND experiments, each layer was recorded 1 minute  
443 before and after the ND. Three consecutive responses to ND were averaged in each layer.  
444 For WIN application, a micropipette was filled with 300  $\mu\text{M}$  WIN solution and placed 100–  
445 150  $\mu\text{m}$  away from the tissue (layer 5), and a pressure pulse at 1 bar (PMI-100 DAGAN,  
446 Minneapolis, MN) was applied for 5 s. The absence of mechanical movement of the tissue  
447 was confirmed in every case. For acute application of CNO, a micropipette was filled with 1  
448 mM CNO solution and placed 100–150  $\mu\text{m}$  away from the recording neuron, and a pressure  
449 pulse was applied for 5 s. The absence of mechanical movement of the tissue was confirmed  
450 in every case. Stimulus effects on EPSCs were statistically tested comparing the normalized  
451 EPSCs recorded 1 min before and 30 s after the stimulus to assess changes in EPSC amplitude  
452 and PPR. Astrocytic  $\text{Ca}^{2+}$  events were recorded at the same time. The changes on the  $\text{Ca}^{2+}$   
453 event probability after CNO application were statistically tested comparing the basal  $\text{Ca}^{2+}$   
454 event probability 1 minute before and 5 s after the stimulus.

455 The effects of pharmacological agents (CPT 5  $\mu\text{M}$  and AM251 2  $\mu\text{M}$ ) were tested after  
456 10 min bath perfusion in the same region and same astrocytes recorded in control conditions.  
457 In the cases when  $\text{Ca}^{2+}$  imaging and electrophysiology were performed at same time the  
458 effects of pharmacological agents were tested at < 40 min after entering whole-cell mode in  
459 the stimulating or recorded neuron.

460

## 461 **AAV viral surgeries**

462 Animals were anesthetized using a ketamine (10 mg/mL) xylazine (1 mg/mL) mixture  
463 and placed on a heating pad to maintain body temperature and faux tears were applied to the  
464 cornea. Animals (8 weeks of age) were placed in a stereotaxic apparatus and an incision was  
465 made down the midline of the scalp to expose the skull. A hole was drilled over the forelimb  
466 and hindlimb somatosensory cortex (S1:  $-0.4_{a-p}$ ,  $1.9_{m-l}$ ), and a Hamilton syringe was lowered  
467 to (in mm from bregma:  $-0.7_{d-v}$ ) and viruses were injected bilaterally at 100 nL/min<sup>48</sup>. Mice  
468 were then sutured and left to heal for 2–3 weeks.

469 AAV5-pZac2.1-gfaABC1d-cyto-GCaMP6f (Addgene), AAV8-GFAP-hM3D(Gq)-  
470 mCherry (UMN vector core), AAV8-GFAP-mCherry (UMN vector core) and AAV8-GFAP-  
471 mCherry-Cre (UMN vector core) viral constructs were used. For CNO experiments,  
472 C57BL/6J mice were injected with AAV8-GFAP-hM3D(Gq)-mCherry virus. In control  
473 conditions, a virus of AAV8-GFAP-mCherry was injected instead. For CB<sub>1</sub>R<sup>fl/fl</sup> mice  
474 experiments, AAV8-GFAP-mCherry-Cre was injected to delete CB<sub>1</sub>R from astrocytes  
475 (aCB<sub>1</sub>R<sup>-/-</sup>). AAV8-GFAP-mCherry was used as a control (aCB<sub>1</sub>R).

476

## 477 **Immunohistochemistry**

478 The animals were anesthetized with Avertin (2,2,2 tribromoethanol, 240 mg/kg, i.p.) and  
479 intracardially perfused with ice cold phosphate buffered saline (PBS) and subsequently with  
480 4% paraformaldehyde (PFA) in 0.1 M phosphate buffered saline (pH 7.4). The brain was  
481 removed, and 100 um coronal sections were made using a Leica VT1000S vibratome.  
482 Vibratome sections were incubated for one h in blocking buffer (0.1% Triton X-100, 10%  
483 Donkey or Goat serum in PBS) at room temperature. The primary antibodies were diluted in  
484 the blocking solution and the sections were incubated for two days at 4°C. The following  
485 primary antibodies were used: Rabbit anti-GFAP (Sigma, 1:500) Mouse anti-NeuN  
486 (Millipore, 1:500). The slices were then washed three times for fifteen minutes each in PBS.  
487 The secondary antibodies were diluted in the secondary antibody buffer (0.1% Triton X-100,  
488 5% Donkey or Goat serum in PBS) and incubated for 2 days at room temperature. The  
489 following secondary antibodies were used: 488 goat anti-rabbit (Invitrogen, 1:1000), 405  
490 goat anti-mouse (Invitrogen, 1:500). The sections were then washed 3 times with 1xPBS for  
491 10 min each and mounted using Vectashield Mounting media (Vector laboratories). The

492 slides were imaged using a Leica SP5 multiphoton confocal microscope and Olympus  
493 FluoView FV1000.

494 The cellular specificity of Cre viral vectors was tested by immunohistochemical analysis of  
495 randomly selected areas of the S1. Out of the 784 cells expressing mCherry from the AAV8-  
496 GFAP-mCherry-Cre viral vector, 86.7% were astrocytes (identified by GFAP) and 11.3%  
497 were neurons (identified by NeuN) (**Figures S2A and S2B**).

498

#### 499 **Biocytin-stained neurons**

500 Pair of neurons were recorded with patch pipettes and filled with internal solution  
501 containing 0.5% biocytin. Slices were fixed in 4% PFA in 0.1 PBS (pH 7.4) at 4°C. Slices  
502 were washed three times in 1xPBS (10 min each). To visualize biocytin slices were incubated  
503 with Alexa488-Streptavidin (RRID: AB 2315383; 1:500) for 48 h at 4°C. Slices were then  
504 washed for 3 times with 1xPBS (10 min each) and mounted with Vectashield mounting media  
505 (Vector laboratories). All mounted slices were imaged using a Leica SP5 multi-photon  
506 microscope. Also, pair of neurons were filled with biocytin through whole-cell recording, the  
507 slices were fixed using 4% paraformaldehyde. Then the slices were washed with PBS (100  
508 mM sodium phosphate, pH 7.2). Endogenous peroxidases were then quenched by incubation  
509 with 1% H<sub>2</sub>O<sub>2</sub>. The slices were subsequently rinsed in PBS. Slices were conjugated with  
510 avidin-biotinylated horseradish peroxidase following the manufacturer's instructions (ABC-  
511 Elite, Vector stains). Slices were then washed, and subsequently, biocytin-stained neurons  
512 were visualized under a reaction with 0.5 mg/ml DAB and 0.01% H<sub>2</sub>O<sub>2</sub>. When the neuronal  
513 processes were visible, the reaction was stopped by washing with PBS.

514

#### 515 **Drugs and Chemicals**

516 4-[3-[2-(Trifluoromethyl)-9H-thioxanthen-9-ylidene]propyl]-1-piperazineethanol  
517 dihydrochloride (flupenthixol dihydrochloride), [S-(R\*,R\*)]-[3-[[1-(3,4-  
518 Dichlorophenyl)ethyl]amino]-2-hydroxypropyl](cyclohexylmethyl) phosphinic acid (CGP  
519 54626 hydrochloride), 8,8'-[Carbonylbis[imino-3,1-phenylenecarbonylimino(4-methyl-3,1-  
520 phenylene)carbonylimino]]bis-1,3,5-naphthalenetrisulfonic acid hexasodium salt (suramin  
521 hexasodium salt), N-(Piperidin-1-yl)-5-(4-iodophenyl)-1-(2,4-dichlorophenyl)-4-methyl-  
522 1H-pyrazole-3-carboxamide (AM251), D-(-)-2-Amino-5-phosphonopentanoic acid (D-

523 AP5), 6-Cyano-7-nitroquinoxaline-2,3-dione disodium (CNQX disodium salt), (S)-(+)-a-  
524 Amino-4-carboxy-2-methylbenzeneacetic acid (LY367385), and 2-Methyl-6-  
525 (phenylethynyl)pyridine hydrochloride (MPEP hydrochloride), Octahydro-12-  
526 (hydroxymethyl)-2-imino-5,9:7,10a-dimethano-10aH-[1,3]dioxocino[6,5-d] pyrimidine-  
527 4,7,10,11,12-pentol (Tetrodotoxin: TTX) were purchased from Tocris Bioscience. Endo-(±)-  
528 α-(Hydroxymethyl)benzeneacetic acid 8-methyl-8-azabicyclo[3.2.1]oct-3-yl ester (atropine)  
529 and 8-Cyclopentyl-1,3-dimethylxanthine (CPT) were from Sigma. Picrotoxin from Indofine  
530 Chemical Company (Hillsborough, NJ). All other drugs were purchased from Sigma.

531

### 532 **Statistical analysis**

533 Number of neurons was used as a sample size for electrophysiology comparisons and  
534 number of slices for Ca<sup>2+</sup> signal comparisons. At least 2 mice per experimental group were  
535 used. Data are expressed as mean ± standard error of the mean (SEM). Data normality was  
536 tested using a Shapiro-Wilk test. Results were compared using a two-tailed Student's t test  
537 (Paired, before-after stimulus-treatment; Unpaired between groups). A full report of the  
538 statistics used in every case is detailed in **Table S1**. Statistical differences were established  
539 with  $p < 0.05$  (\*),  $p < 0.01$  (\*\*) and  $p < 0.001$  (\*\*\*)).

540

541

### 542 **ACKNOWLEDGMENTS**

543 We would like to thank Dana Deters for technical support. We thank Carmen Nanclares, José  
544 Noriega, Francisco Emmanuel Labrada-Moncada, Julianna Goenaga, Carlos García, Pavan  
545 Guttipatti, Grace Gall and Jessica Neamtu helpful suggestions. We thank Justin Lines for  
546 providing Calsee and for helpful suggestions. We thank Guillermo Marques and Jason  
547 Mitchell at the University of Minnesota – University Imaging Centers for assistance using  
548 the Leica SP5 multiphoton upright microscope. We thank J. Chen (UCSD, USA) for  
549 providing IP<sub>3</sub>R<sub>2</sub> mice. We thank the University of Minnesota Viral Vector and Cloning Core  
550 for production of some of the viral vectors used in this study. This work was supported by a  
551 postdoctoral fellowship from Basque Government, Spain, to AMB; grants from National  
552 Institutes of Health (NIH-MH R01MH119355; NIH-NINDS R01NS097312; and NIH-NIDA

553 R01DA048822) to AA and grants from FEDER and ISCIII (AES2018-PI18/00513) and the  
554 Basque Government (PIBA19-0059) to SM, and ARSEP Foundation to SM and GM.

555 **AUTHOR CONTRIBUTIONS**

556 A.M.B. performed experiments and analyzed data. L.B. and P.K. performed  
557 immunohistochemistry. P.K., A.A., G.M., C.M., S.M. and A.M.B. conceived the study and  
558 wrote the manuscript.

559 **COMPETING FINANCIAL INTERESTS**

560 The authors declare no competing financial interests.

## REFERENCES

1. Lorente de Nó, R. Studies on the structure of the cerebral cortex I The area entorhinalis. *J. Psychol. Neurol.* **45**, 381–438 (1933).
2. Lorente de No, R. Architectonics and structure of the cerebral cortex. in *Physiology of the Nervous System* 291–330 (New York: Oxford University Press, 1938).
3. Mountcastle, V. The columnar organization of the neocortex. *Brain* **120**, 701–722 (1997).
4. DeFelipe, J. The neocortical column. *Front. Neuroanat.* **6**, (2012).
5. Markram, H. Fixing the location and dimensions of functional neocortical columns. *HFSP Journal* **2**, 132–135 (2008).
6. Harris, K. D. & Shepherd, G. M. G. The neocortical circuit: themes and variations. *Nat. Neurosci.* **18**, 170–181 (2015).
7. Perea, G., Navarrete, M. & Araque, A. Tripartite synapses: astrocytes process and control synaptic information. *Trends in Neurosci.* **32**, 421–431 (2009).
8. Araque, A. *et al.* Gliotransmitters Travel in Time and Space. *Neuron* **81**, 728–739 (2014).
9. Volterra, A., Liaudet, N. & Savtchouk, I. Astrocyte Ca<sup>2+</sup> signalling: an unexpected complexity. *Nat. Rev. Neurosci.* **15**, 327–335 (2014).
10. Wang, X. *et al.* Astrocytic Ca<sup>2+</sup> signaling evoked by sensory stimulation in vivo. *Nat. Neurosci.* **9**, 816–823 (2006).
11. Schummers, J., Yu, H. & Sur, M. Tuned Responses of Astrocytes and Their Influence on Hemodynamic Signals in the Visual Cortex. *Science* **320**, 1638–1643 (2008).
12. Benedetti, B., Matyash, V. & Kettenmann, H. Astrocytes control GABAergic inhibition of neurons in the mouse barrel cortex: Astrocytes inhibit cortical neurons. *J. Physiol.* **589**, 1159–1172 (2011).
13. Takata, N. *et al.* Astrocyte Calcium Signaling Transforms Cholinergic Modulation to Cortical Plasticity In Vivo. *J. Neurosci.* **31**, 18155–18165 (2011).
14. Schipke, C. G., Haas, B. & Kettenmann, H. Astrocytes Discriminate and Selectively Respond to the Activity of a Subpopulation of Neurons within the Barrel Cortex. *Cereb. Cortex* **18**, 2450–2459 (2008).
15. Min, R. & Nevian, T. Astrocyte signaling controls spike timing–dependent depression at neocortical synapses. *Nat. Neurosci.* **15**, 746–753 (2012).
16. Perez-Alvarez, A., Navarrete, M., Covelo, A., Martin, E. D. & Araque, A. Structural and Functional Plasticity of Astrocyte Processes and Dendritic Spine Interactions. *J. Neurosci.* **34**, 12738–12744 (2014).
17. Lines, J., Martin, E. D., Kofuji, P., Aguilar, J. & Araque, A. Astrocytes modulate sensory-evoked neuronal network activity. *Nat. Commun.* **11**, 3689 (2020).
18. Ghosh, A., Wyss, M. T. & Weber, B. Somatotopic astrocytic activity in the somatosensory cortex. *Glia* **61**, 601–610 (2013).
19. Poskanzer, K. E. & Yuste, R. Astrocytic regulation of cortical UP states. *Proc. Natl. Acad. Sci. USA* **108**, 18453–18458 (2011).
20. Poskanzer, K. E. & Yuste, R. Astrocytes regulate cortical state switching in vivo. *Proc. Natl. Acad. Sci. USA* **113**, E2675–E2684 (2016).
21. Lines, J. *et al.* Astrocyte-neuronal network interplay is disrupted in Alzheimer’s disease mice. *Glia* **70**, 368–378 (2021).
22. Navarrete, M. & Araque, A. Endocannabinoids Potentiate Synaptic Transmission through Stimulation of Astrocytes. *Neuron* **68**, 113–126 (2010).

23. Zhang, J. *et al.* ATP Released by Astrocytes Mediates Glutamatergic Activity-Dependent Heterosynaptic Suppression. *Neuron* **40**, 971–982 (2003).
24. Pascual, O. *et al.* Astrocytic Purinergic Signaling Coordinates Synaptic Networks. *Science* **310**, 113–116 (2005).
25. Covelo, A. & Araque, A. Lateral regulation of synaptic transmission by astrocytes. *Neuroscience* **323**, 62–66 (2016).
26. Han, J. *et al.* Acute Cannabinoids Impair Working Memory through Astroglial CB1 Receptor Modulation of Hippocampal LTD. *Cell* **148**, 1039–1050 (2012).
27. Gómez-Gonzalo, M. *et al.* Endocannabinoids Induce Lateral Long-Term Potentiation of Transmitter Release by Stimulation of Gliotransmission. *Cereb. Cortex* **25**, 3699–3712 (2015).
28. Ohno-Shosaku, T., Maejima, T. & Kano, M. Endogenous Cannabinoids Mediate Retrograde Signals from Depolarized Postsynaptic Neurons to Presynaptic Terminals. *Neuron* **29**, 729–738 (2001).
29. Wilson, R. I. & Nicoll, R. A. Endogenous cannabinoids mediate retrograde signalling at hippocampal synapses. *Nature* **410**, 588–592 (2001).
30. Chevaleyre, V. & Castillo, P. E. Heterosynaptic LTD of Hippocampal GABAergic Synapses. *Neuron* **38**, 461–472 (2003).
31. Chevaleyre, V. & Castillo, P. E. Endocannabinoid-Mediated Metaplasticity in the Hippocampus. *Neuron* **43**, 871–881 (2004).
32. Piomelli, D. The molecular logic of endocannabinoid signalling. *Nat. Rev. Neurosci.* **4**, 873–884 (2003).
33. Castillo, P. E., Younts, T. J., Chávez, A. E. & Hashimoto, Y. Endocannabinoid Signaling and Synaptic Function. *Neuron* **76**, 70–81 (2012).
34. Diana, M. A. & Marty, A. Endocannabinoid-mediated short-term synaptic plasticity: depolarization-induced suppression of inhibition (DSI) and depolarization-induced suppression of excitation (DSE): DSI/DSE: two forms of CB1R-mediated plasticity. *Br. J. Pharmacol.* **142**, 9–19 (2004).
35. Navarrete, M. & Araque, A. Endocannabinoids Mediate Neuron-Astrocyte Communication. *Neuron* **57**, 883–893 (2008).
36. Martin-Fernandez, M. *et al.* Synapse-specific astrocyte gating of amygdala-related behavior. *Nat. Neurosci.* **20**, 1540–1548 (2017).
37. Corkrum, M. *et al.* Dopamine-Evoked Synaptic Regulation in the Nucleus Accumbens Requires Astrocyte Activity. *Neuron* **105**, 1036–1047.e5 (2020).
38. Navarrete, M. *et al.* Astrocytes Mediate In Vivo Cholinergic-Induced Synaptic Plasticity. *PLoS Biol* **10**, e1001259 (2012).
39. Di Castro, M. A. *et al.* Local Ca<sup>2+</sup> detection and modulation of synaptic release by astrocytes. *Nat. Neurosci.* **14**, 1276–1284 (2011).
40. Petrávicz, J., Fiacco, T. A. & McCarthy, K. D. Loss of IP3 Receptor-Dependent Ca<sup>2+</sup> Increases in Hippocampal Astrocytes Does Not Affect Baseline CA1 Pyramidal Neuron Synaptic Activity. *J. Neurosci.* **28**, 4967–4973 (2008).
41. Panatier, A. *et al.* Astrocytes Are Endogenous Regulators of Basal Transmission at Central Synapses. *Cell* **146**, 785–798 (2011).
42. Serrano, A. GABAergic Network Activation of Glial Cells Underlies Hippocampal Heterosynaptic Depression. *J. Neurosci.* **26**, 5370–5382 (2006).
43. Covelo, A. & Araque, A. Neuronal activity determines distinct gliotransmitter release from a single astrocyte. *eLife* **7**, e32237 (2018).

44. Houades, V., Koulakoff, A., Ezan, P., Seif, I. & Giaume, C. Gap Junction-Mediated Astrocytic Networks in the Mouse Barrel Cortex. *J. Neurosci.* **28**, 5207–5217 (2008).
45. Eilam, R., Aharoni, R., Arnon, R. & Malach, R. Astrocyte morphology is confined by cortical functional boundaries in mammals ranging from mice to human. *eLife* **5**, e15915 (2016).
46. Marsicano, G. *et al.* CB1 Cannabinoid Receptors and On-Demand Defense Against Excitotoxicity. *Science* **302**, 84–88 (2003).
47. Li, X., Zima, A. V., Sheikh, F., Blatter, L. A. & Chen, J. Endothelin-1–Induced Arrhythmogenic  $\text{Ca}^{2+}$  Signaling Is Abolished in Atrial Myocytes of Inositol-1,4,5-Trisphosphate ( $\text{IP}_3$ )–Receptor Type 2–Deficient Mice. *Circ. Res.* **96**, 1274–1281 (2005).
48. Paxinos, G., F., K. *Paxinos and Franklin's the Mouse Brain in Stereotaxic Coordinates.* (Elsevier B.V., 2012).



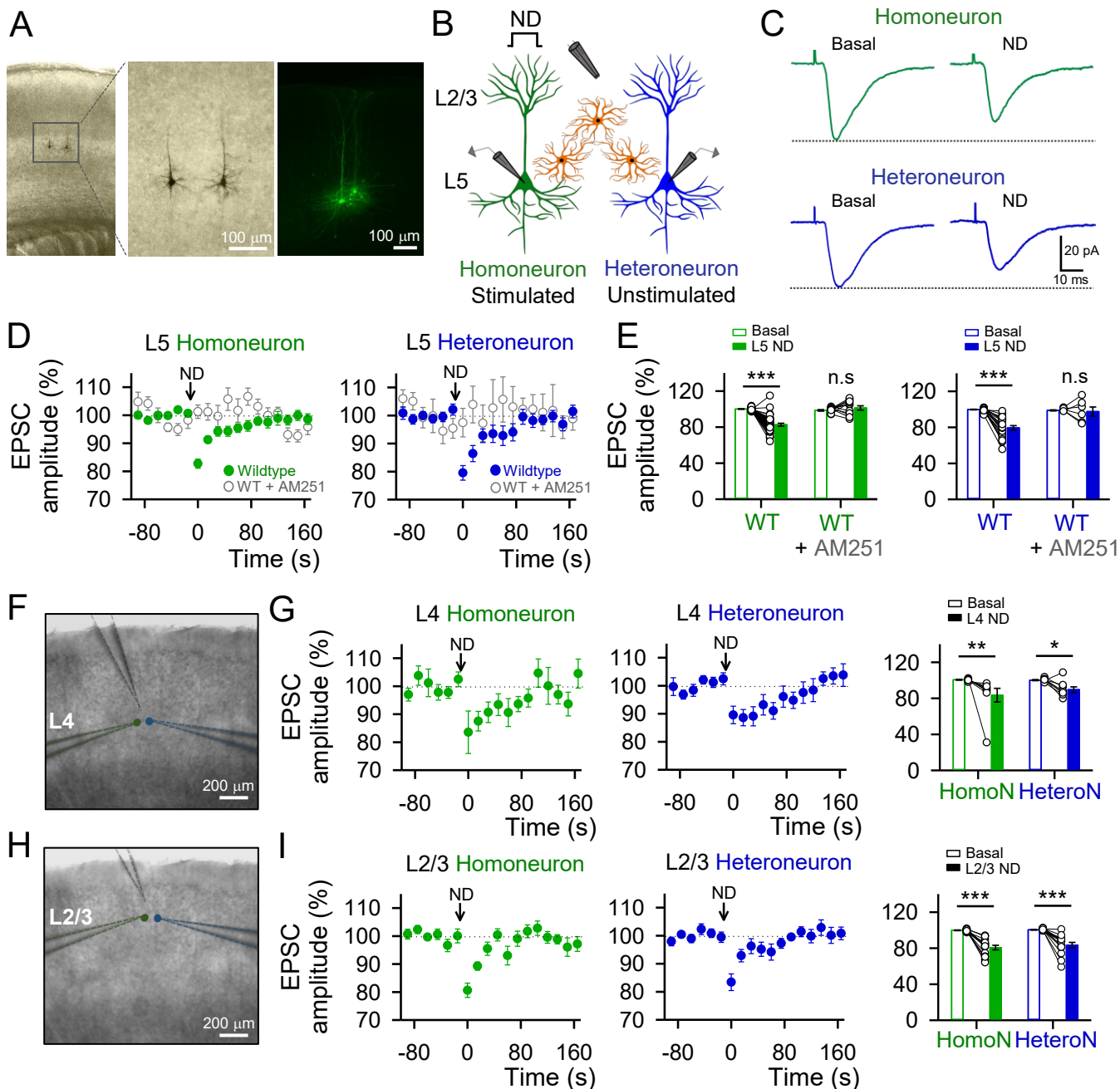


**Figure 1. Endocannabinoid signaling induces homoneuronal and heteroneuronal synaptic depression in S1**

(A) Biocytin loading S1 L5 pyramidal neurons image. (B) Schematic drawing depicting double patch-recordings from L5 pyramidal neurons and the stimulating electrode in L2/3. (C) Averaged EPSCs ( $n = 20$  stimuli) before (control) and after neuronal depolarization (ND) in wildtype mice. (D) EPSCs amplitude *versus* time before (basal) and after ND in control (green or blue) and in the presence of AM251 ( $2 \mu\text{M}$ ; open grey) in the homoneuron (left) and heteroneuron (right) from layer 5. (E) Relative changes in EPSC amplitude in control and with AM251 ( $2 \mu\text{M}$ ). Two-tailed Student's paired t test. (F) Representative infrared differential interference contrast image of the experimental configuration with the stimulation pipette in layer 4 and the homoneuronal and heteroneuronal neurons located in layer 4. (G) EPSCs amplitude *versus* time before (basal) and after ND in the homoneuron (left, green) and heteroneuron (middle, blue) in the experimental conditions represented in panel F. Right: Relative changes in EPSC amplitude. (H) Representative infrared differential interference contrast image of the experimental configuration with the stimulation pipette in L2/3 and the homoneuronal and heteroneuronal neurons located in L2/3. (I) EPSCs amplitude *versus* time before (basal) and after ND in the homoneuron (left, green) and heteroneuron (middle, blue) in the experimental conditions represented in panel H. Right: Relative changes in EPSC amplitude. Two-tailed Student's paired t test. Data are expressed as mean  $\pm$  SEM, \* $p < 0.05$ , \*\* $p < 0.01$ , \*\*\* $p < 0.001$ .

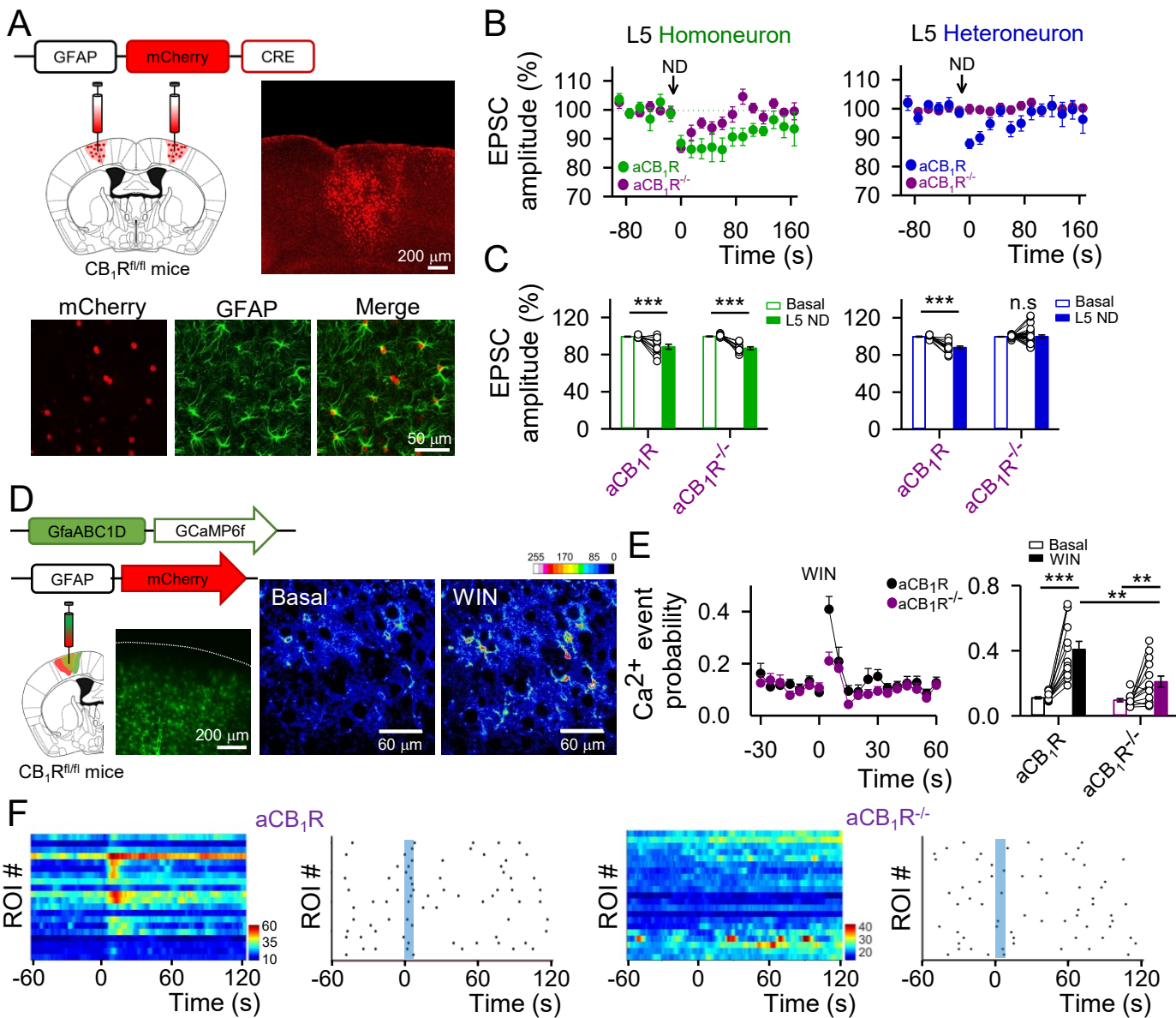


**Figure 2. Heteroneuronal, but not homoneuronal, synaptic depression requires endocannabinoid signaling in astrocytes**

(A) Viral vector injected into the S1 of CB<sub>1</sub>R<sup>fl/fl</sup> mice and fluorescence image showing mCherry-Cre expression in the S1 (top), and immunohistochemistry images showing co-localization between mCherry-cre and GFAP (bottom). (B) EPSCs amplitude *versus* time before (basal) and after ND in CB<sub>1</sub>R mice injected with AAV8-GFAP-mCherry (aCB<sub>1</sub>R; green or blue) or with AAV8-GFAP-mCherry-Cre (aCB<sub>1</sub>R<sup>-/-</sup>; purple) in the homoneuron (left) and heteroneuron (right) from L5. (C) Relative changes in EPSC amplitude in aCB<sub>1</sub>R and aCB<sub>1</sub>R<sup>-/-</sup> mice in the homoneuron (left) and heteroneuron (right). Two-tailed Student's paired t test. (D) Viral vector injected into the S1 of CB<sub>1</sub>R<sup>fl/fl</sup> mice, fluorescence image showing GCaMP6f expression in the S1 and pseudocolor images showing the fluorescence intensities of GCaMP6f-expressing astrocytes before and after WIN (300  $\mu$ M) application in L5. (E) Ca<sup>2+</sup> event probability over time (left) and Ca<sup>2+</sup> event probability before (basal) and after WIN application in aCB<sub>1</sub>R (black) and aCB<sub>1</sub>R<sup>-/-</sup> (purple) mice (right). Blue shadow indicates 5s WIN application. Two-tailed Student's paired t test (before and after) and two-tailed Student's unpaired t test (between groups). (F) Raster plots and heat maps showing the Ca<sup>2+</sup> events recorded from all ROIs including astrocyte somas and processes in aCB<sub>1</sub>R (left) and aCB<sub>1</sub>R<sup>-/-</sup> (right) mice before and after WIN stimulation. Blue shadow indicates 5s WIN application. Data are expressed as mean  $\pm$  SEM, \*\*p < 0.01, \*\*\*p < 0.001.

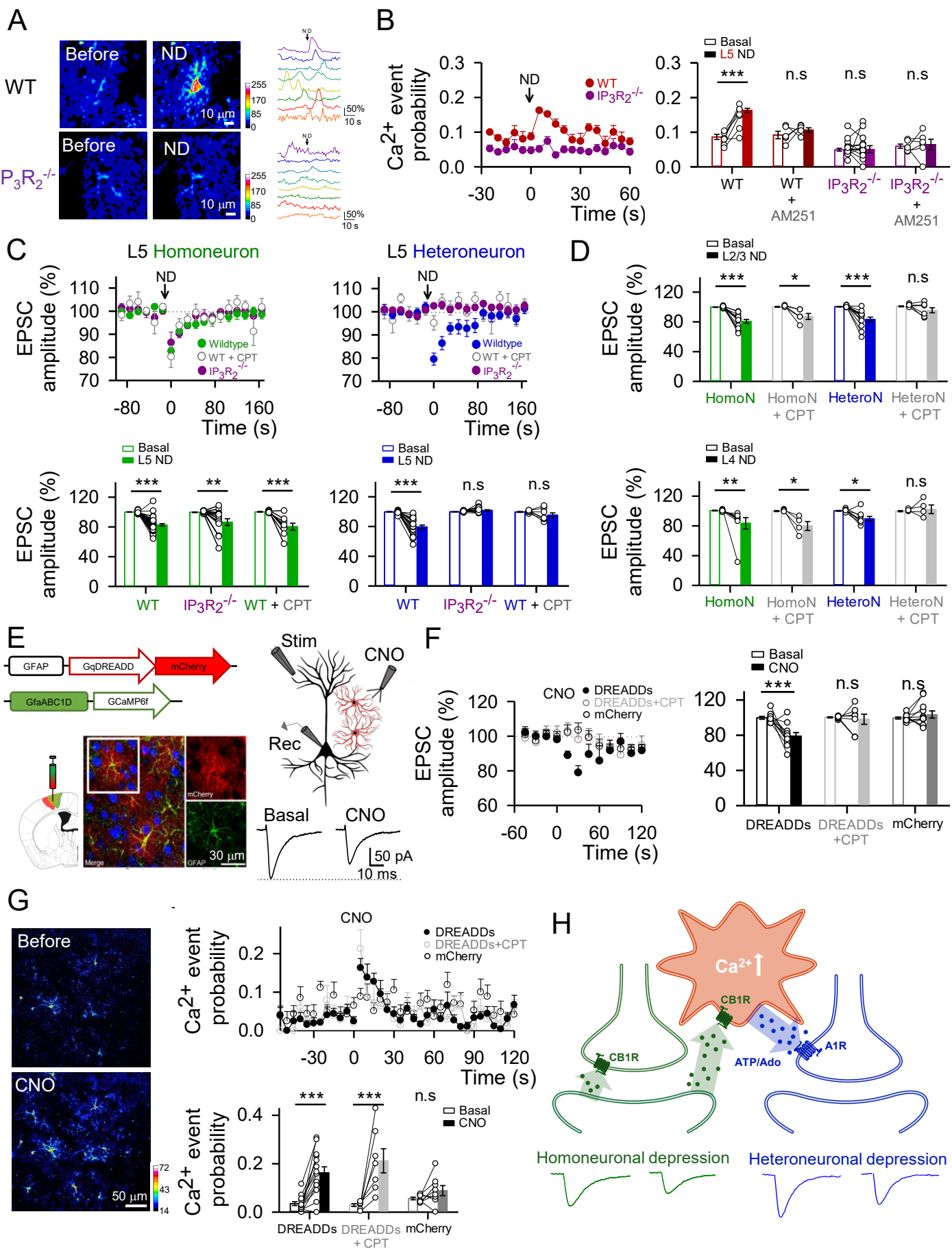
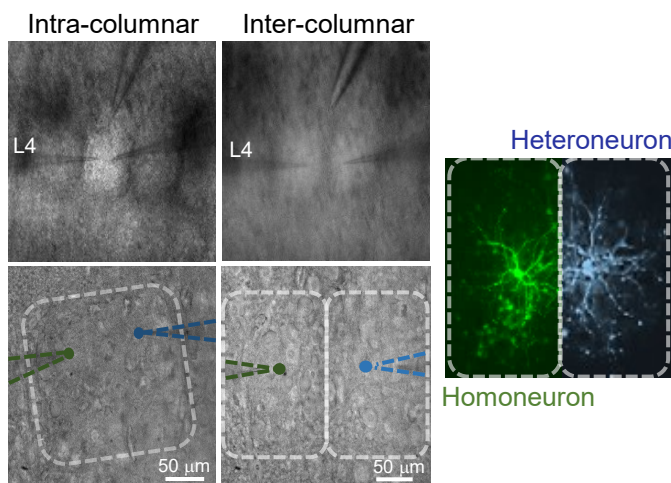


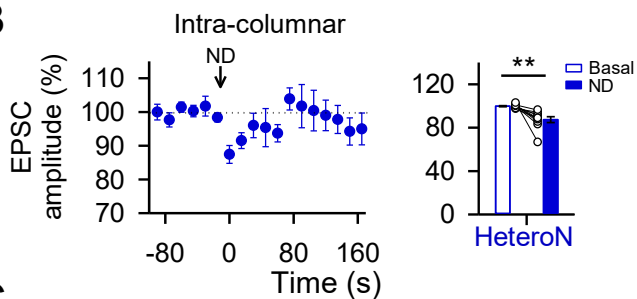
### Figure 3. Heteroneuronal synaptic depression requires astrocyte calcium signaling and activation of presynaptic A1 receptors

(A) Left: Pseudocolor images showing the fluorescence intensities of GCaMP6f-expressing astrocytes in L5 before and after L5 ND in wildtype (top) and  $IP_3R_2^{-/-}$  mice (bottom). Right: representative  $Ca^{2+}$  traces of astrocytes (arrow indicates ND). (B) Left: L5 astrocytes  $Ca^{2+}$  event probability over time before (basal) and after L5 ND in wildtype (red) and  $IP_3R_2^{-/-}$  (purple) mice. Right: Relative changes in  $Ca^{2+}$  event probability in wildtype and  $IP_3R_2^{-/-}$  mice in control and with AM251 (2  $\mu$ M). All experimental conditions were performed in TTX (1  $\mu$ M) and in a cocktail of neurotransmitter receptor antagonists (see Material and Methods). Two-tailed Student's paired t test. (C) Top: EPSCs amplitude *versus* time before (basal) and after ND in wildtype mice in control (green or blue), in presence of CPT (5  $\mu$ M) (open gray) and in  $IP_3R_2^{-/-}$  mice (purple) in the homoneuron (left) and heteroneuron (right) from layer 5. Bottom: Relative changes in EPSC amplitude in wildtype mice in control, in presence of CPT (5  $\mu$ M) and in  $IP_3R_2^{-/-}$  mice. Two-tailed Student's paired t-test. (D) Top: Relative changes in EPSC amplitude before (basal) and after L2/3 ND in control and with CPT (5  $\mu$ M) in the homoneuron (green) and heteroneuron (blue) from layer 2/3. Bottom: Relative changes in EPSC amplitude before (basal) and after L4 ND in control and with CPT (5  $\mu$ M) in the homoneuron (green) and heteroneuron (blue) from layer 4. Two-tailed Student's paired t test. (E) Left: Viral vectors injected into the S1 of wildtype mice and immunohistochemistry images showing the expression of NeuN (blue), mCherry (red) and GFAP (green) in the somatosensory cortex slices of a DREADDs injected mouse. Note the selective expression of hm3D-mCherry in astrocytes. Right: Scheme of the experimental approach and representative EPSC traces before (basal) and after CNO (1mM) application in L5. (F) Left: EPSCs amplitude *versus* time before (basal) and after CNO application in AAV8-GFAP-Gq-DREADD-mCherry injected mice in control (black, close) and in presence of CPT (gray, open), and in AAV8-GFAP-mCherry injected mice (black, open). Blue shadow indicates 5s CNO application. Right: Relative changes in EPSC amplitude in DREADDs injected mice in control and in presence of CPT, and in mCherry injected mice. Two-tailed Student's paired t test. (G) Left: Pseudocolor images showing the fluorescence intensities of GCaMP6f-expressing astrocytes before and after CNO application in L5. Top right:  $Ca^{2+}$  event probability over time of L5 astrocytes before (basal) and after CNO application in AAV8-GFAP-Gq-DREADD-mCherry injected mice in control (black, close) and in presence of CPT (gray, open), and in AAV8-GFAP-mCherry injected mice (black, open). Blue shadow indicates 5s CNO application. Bottom right: relative changes in  $Ca^{2+}$  event probability in DREADDs injected mice in control and in presence of CPT, and in mCherry injected mice. Two-tailed Student's paired t test. (H) Schematic summary depicting the signaling pathways involved in eCBs-induced heteroneuronal synaptic depression. Data are expressed as mean  $\pm$  SEM, \* $p < 0.05$ , \*\* $p < 0.01$ , \*\*\* $p < 0.001$ .

A



B



C

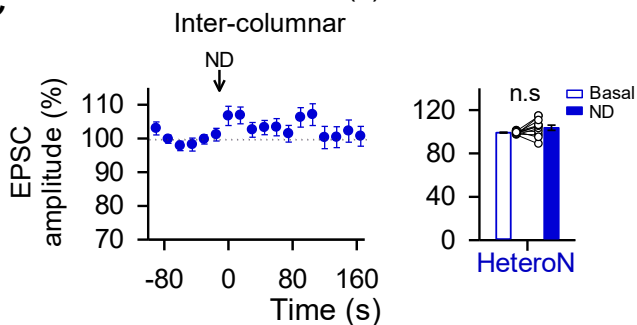
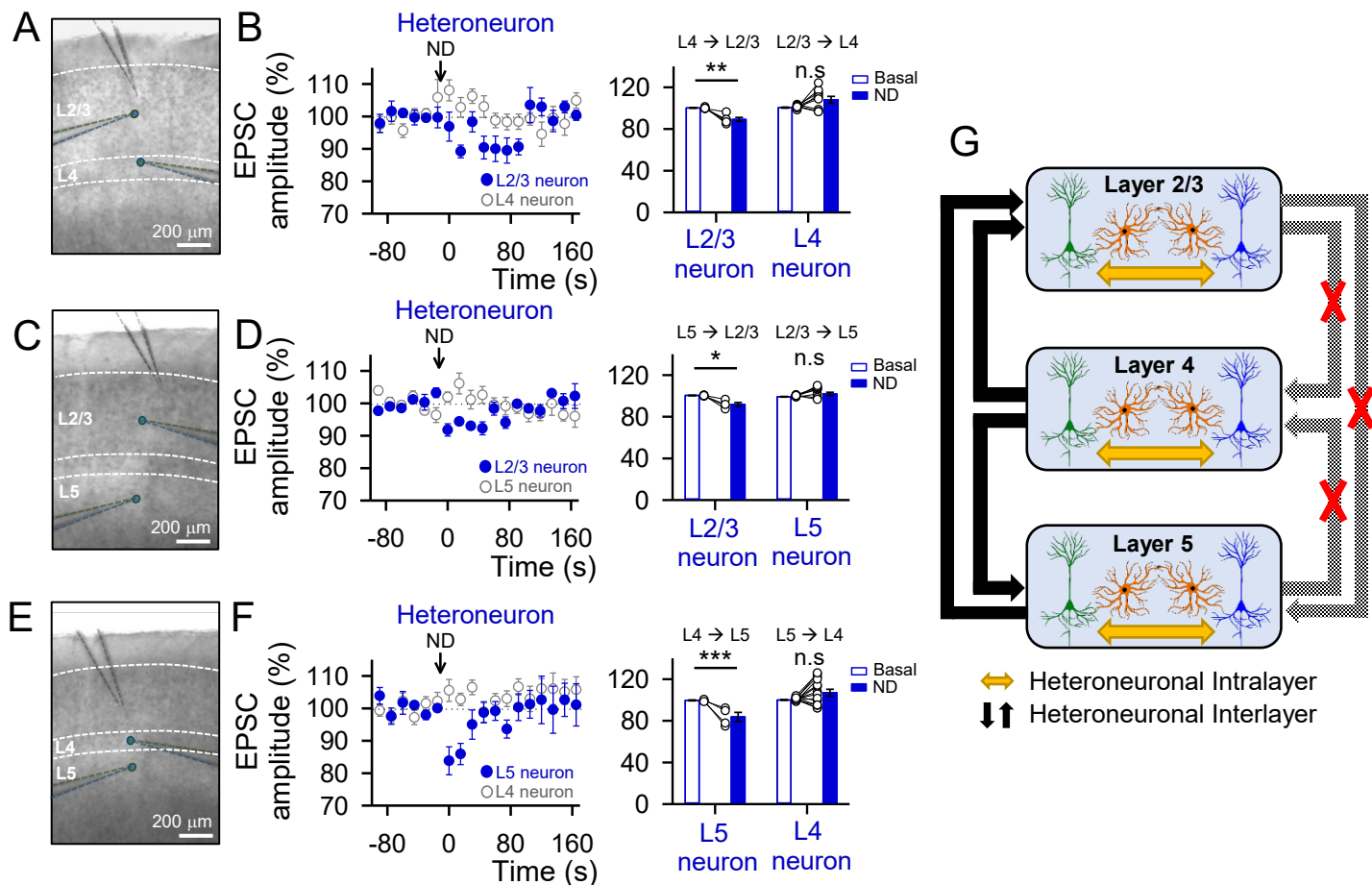


Fig. 4

**Figure 4. Astrocyte-mediated heterosynaptic depression is column specific.**

(A) Representative infrared differential interference contrast images of the barrel field in the primary somatosensory cortex showing intracolumnar (left) and intercolumnar (middle) pair of neurons patched and the stimulation electrode. False-color biocytin loading barrel cortex intercolumnar pair of neurons image (right). (B) Left: EPSCs amplitude *versus* time before (basal) and after ND in the intracolumnar heteroneuron. Right: Relative changes in EPSC amplitude in the intracolumnar heteroneuron. (C) Left: EPSCs amplitude *versus* time before (basal) and after ND in the intercolumnar heteroneuron. Right: Relative changes in EPSC amplitude in the intercolumnar heteroneuron. Two-tailed Student's paired t test. Data are expressed as mean  $\pm$  SEM, \*\* $p < 0.01$ .



**Figure 5. Astrocyte-mediated heterosynaptic depression is layer specific.**

(A) Representative infrared differential interference contrast image of the experimental configuration with the stimulation pipette in layer 2/3 and a pair of neurons patched one in L4 and the other in L2/3. (B) Left: Heterosynaptic EPSCs amplitude versus time in a pair of neurons patched one in L4 and the other in L2/3 before (basal) and after ND of L4 (blue) or L2/3 neuron (open grey). Right: Relative changes in EPSC amplitude in L2/3 (when L4 neuron is stimulated) and L4 (when L2/3 neuron is stimulated) neuron. Two-tailed Student's paired t-test. (C) Representative infrared differential interference contrast image of the experimental configuration with the stimulation pipette in layer 2/3 and a pair of neurons patched one in L5 and the other in L2/3. (D) Left: Heterosynaptic EPSCs amplitude versus time in a pair of neurons patched one in L5 and the other in L2/3 before (basal) and after ND of L5 (blue) or L2/3 neuron (open grey). Right: Relative changes in EPSC amplitude in L2/3 (when L5 neuron is stimulated) and L5 (when L2/3 neuron is stimulated) neuron. Two-tailed Student's paired t-test. (E) Representative infrared differential interference contrast image of the experimental configuration with the stimulation pipette in layer 2/3 and a pair of neurons patched one in L4 and the other in L5. (F) Left: Heterosynaptic EPSCs amplitude versus time in a pair of neurons patched one in L4 and the other in L5 before (basal) and after ND of L4 (blue) or L5 neuron (open grey). Right: Relative changes in EPSC amplitude in L5 (when L4 neuron is stimulated) and L4 (when L5 neuron is stimulated) neuron. Two-tailed Student's paired t test. (G) Schematic summary depicting the astrocyte-mediated heterosynaptic regulation pathways into the same layer (intralayer) and between layers (interlayer). Data are expressed as mean ± SEM, \*p < 0.05, \*\*p < 0.01, \*\*\*p < 0.001.

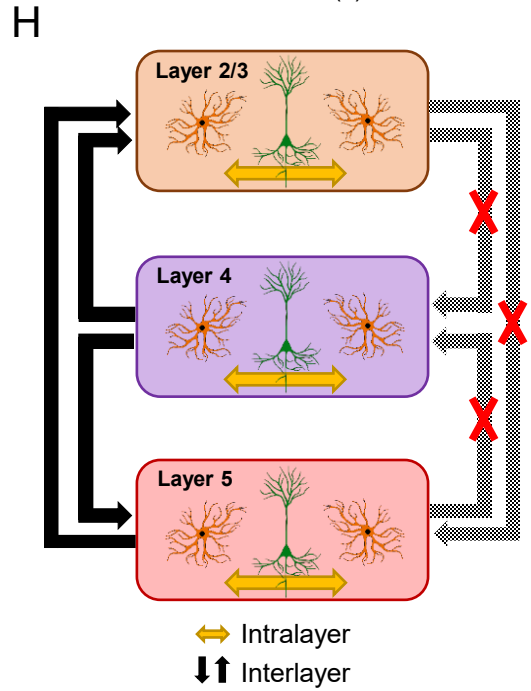
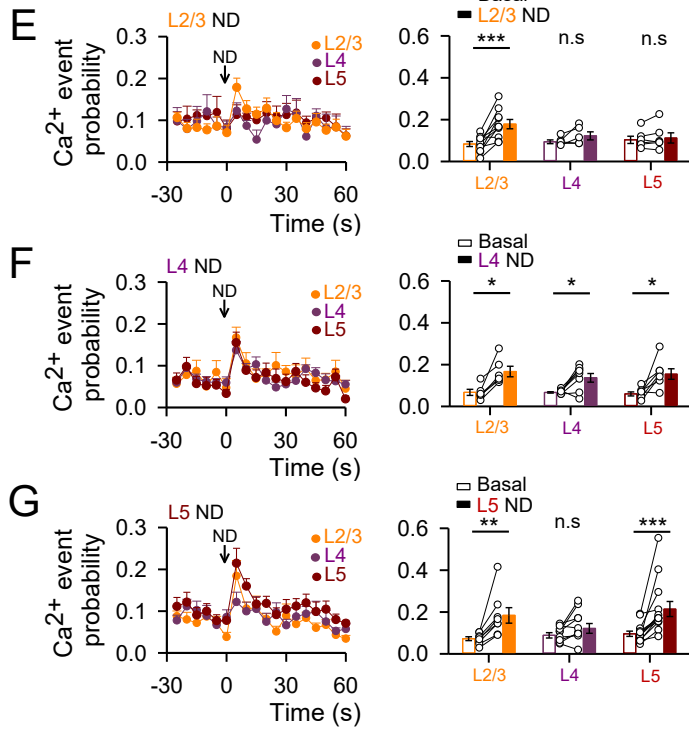
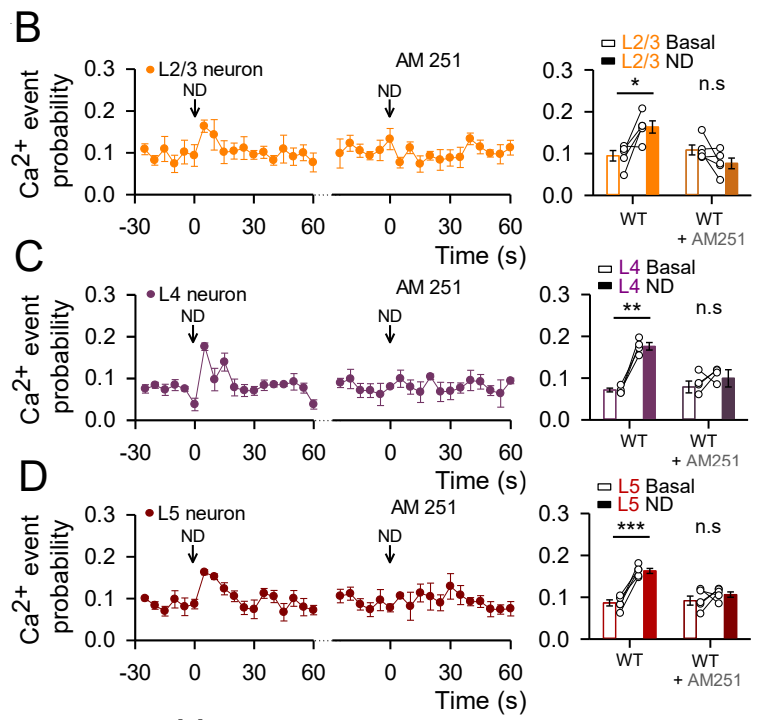
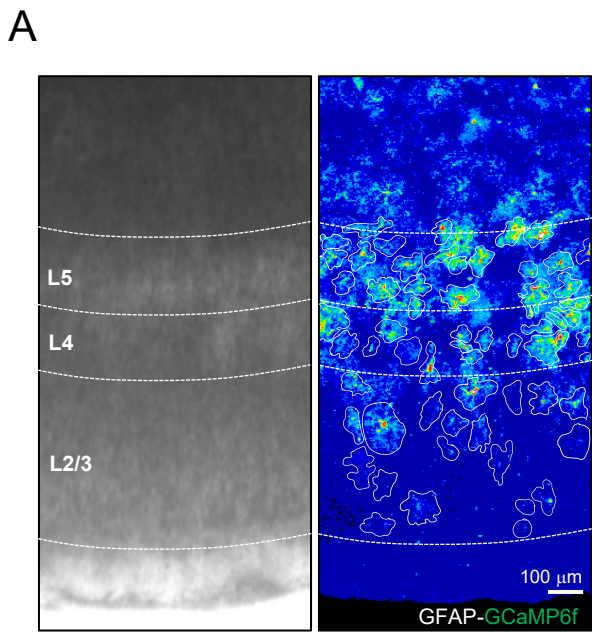


**Figure 6. Astrocytic calcium responses to eCBs are not homogeneous across cortical layers.**

(A) Representative infrared differential interference contrast image and pseudocolor image representing fluorescence intensities of GCaMP6f-expressing astrocytes in the different layers of the primary somatosensory cortex. (B-D) Left:  $\text{Ca}^{2+}$  event probability over time before (basal) and after ND in control and in presence of AM251 (2  $\mu\text{M}$ ) when patched and recorded in L2/3 (B, orange), L4 (C, purple) or L5 (D, red). Right: relative changes in  $\text{Ca}^{2+}$  event probability in control and in presence of AM251 (2  $\mu\text{M}$ ) when patched and recorded in L2/3 (B, orange), L4 (C, purple) or L5 (D, red). Two-tailed Student's paired t test. (E) Left:  $\text{Ca}^{2+}$  event probability over time of astrocytes of layer 2/3 (orange), 4 (purple) and 5 (red) before (basal) and after L2/3 neuron depolarization. Right: relative changes in  $\text{Ca}^{2+}$  event probability of astrocytes of layer 2/3 (orange), 4 (purple) and 5 (red). Two-tailed Student's paired t test. (F) Left:  $\text{Ca}^{2+}$  event probability over time of astrocytes of layer 2/3 (orange), 4 (purple) and 5 (red) before (basal) and after L4 neuron depolarization. Right: relative changes in  $\text{Ca}^{2+}$  event probability of astrocytes of layer 2/3 (orange), 4 (purple) and 5 (red). Two-tailed Student's paired t test. (G) Left:  $\text{Ca}^{2+}$  event probability over time of astrocytes of layer 2/3 (orange), 4 (purple) and 5 (red) before (basal) and after L5 neuron depolarization. Right: relative changes in  $\text{Ca}^{2+}$  event probability of astrocytes of layer 2/3 (orange), 4 (purple) and 5 (red). Two-tailed Student's paired t test. All experimental conditions were performed in TTX (1  $\mu\text{M}$ ) and in a cocktail of neurotransmitter receptor antagonists (see Material and Methods). (H) Schematic summary depicting the calcium responses of astrocytes located in the same (intralayer) or different (interlayer) layers to the endogenous mobilized eCBs from neurons located in the same or different layers. Data are expressed as mean  $\pm$  SEM, \* $p < 0.05$ , \*\* $p < 0.01$ , \*\*\* $p < 0.001$ .